

Magnetic Electron Configuration in Iron*

C. G. SHULL

Massachusetts Institute of Technology, Cambridge, Massachusetts

Introduction

About two years ago, a research program directed at the determination of the slow neutron magnetic scattering amplitudes of iron was started by Dr. F. P. Ricci and the author, followed by extensive work by Dr. Y. Yamada. The polarized neutron technique has been used in these studies whereby it is possible to determine the amplitudes accurately to large scattering angles. A knowledge of the magnetic scattering amplitudes can be used to establish the spatial distribution of the magnetic electrons and to correlate this with the spin and orbital moment contributions to the magnetization of the $3d$ and other electron groups. Additionally the amplitudes can be Fourier transformed to yield directly the distribution of the localized magnetization throughout the unit cell.

Previous measurements on the magnetic scattering amplitudes associated with five crystal reflections of iron have been reported by Nathans et al.¹ Although the data were sparse, they have been interpreted by Weiss and Freeman² as suggesting the presence of a slight departure from spherical symmetry for the $3d$ -electrons with favoritism toward the E_g rather than the T_{2g} configuration. In the cubic field surrounding an iron atom, the d -electron charge distributions are expected to reside in two configuration sets, E_g with concentration along the $[100]$ cube edges and T_{2g} with concentration along the $[111]$ cube diagonals.

Experimental Results

All of the crystal reflections out to the (622) reflection from pure iron crystals have been studied corresponding to a maximum $\sin \theta/\lambda$ value of 1.157 \AA^{-1} . The magnetic scattering amplitude for each reflection is obtained in absolute value with the polarized beam technique, and this has been converted to the magnetic form factor value by normalization

* This research was supported by the U. S. National Science Foundation.

relative to the amplitude at zero scattering angle as calculated from the iron magnetization. Figure 1 illustrates the form factor values for the 26 reflections which have been studied with the size of the experimental points representing the accuracy of the individual determinations. For comparison purposes there is also shown in Figure 1 the spherical atom form factor as calculated by Watson and Freeman³ for the magnetic spin density to be expected for the two configurations $3d^8$ and $3d^64s^2$.

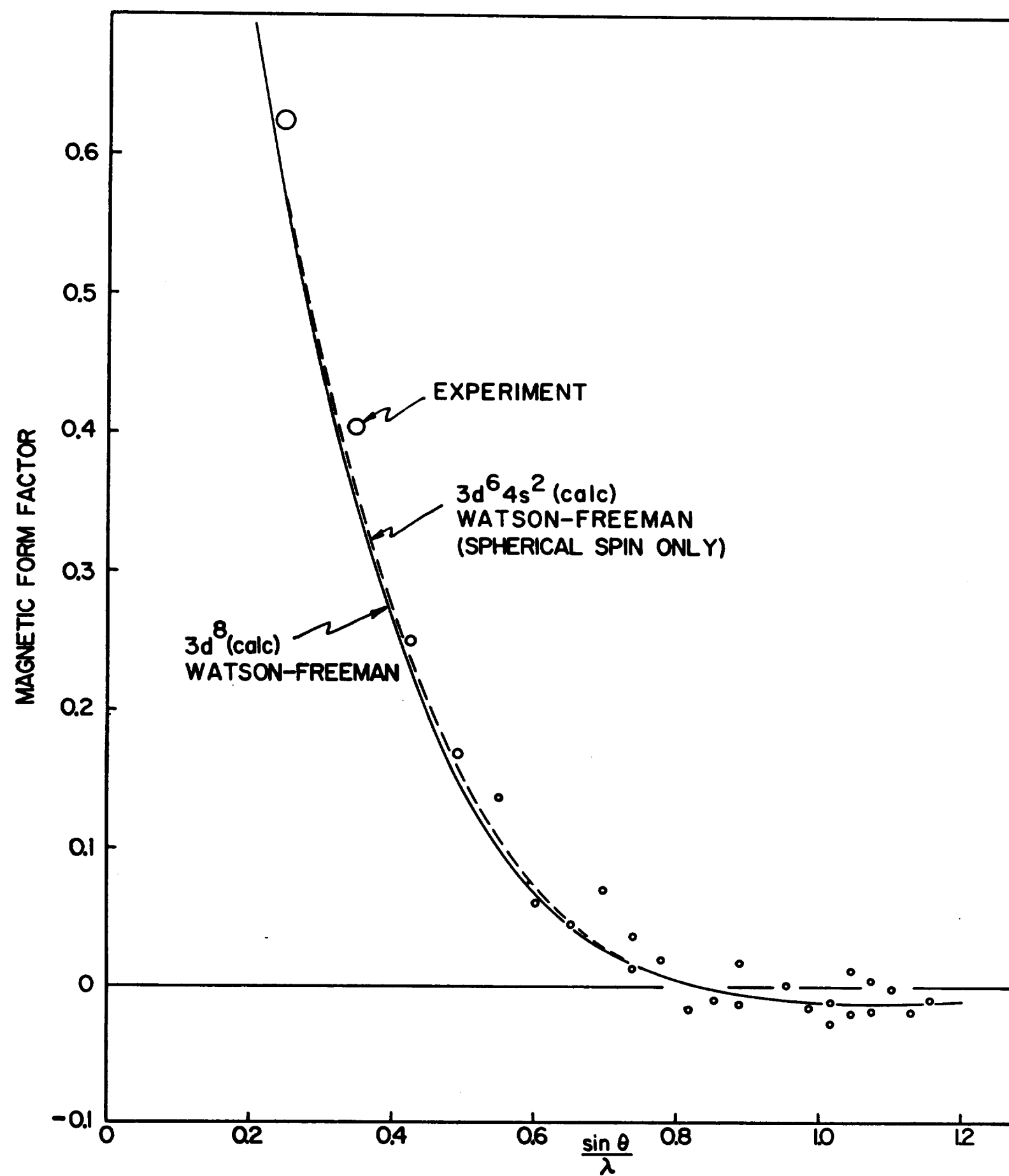


Fig. 1. Comparison between experimental and calculated values of the magnetic form factor for iron. The calculated curves are representative of the spherically symmetric spin density in the $3d$ electrons of free atoms.

These calculations are free atom Hartree-Fock calculations with exact exchange-polarization treatment.

It is seen that the range of the experimental observations includes a considerable number of negative form factor reflections, the sign being obtained directly from the polarized beam intensities. Included in the observations are five pairs of reflections for which the scattering angle is the same within the pair. Such paired reflections are interesting because the noticeably different form factors show directly that the form factor is directionally sensitive and hence that *the magnetic electron density is not spherically symmetric around the nucleus*. This is emphasized in Figure 1 by the comparison with the calculated spherical atom form factors. The data points deviate from either of the curves by as much as 10 times experimental error depending upon the crystal direction which is sampled in a given reflection.

Magnetic Form Factor Interpretation

In the detailed comparison of the observed form factor points with calculated values, allowance must be made for the 3*d*-orbital moment scattering along with possible form factor contributions from other electron groups. There will be both quenched and unquenched moment contributions to the 3*d* magnetization, and the relative amounts of these can be evaluated from the experimental magnetomechanical ratio of 1.93. Watson and Freeman³ have calculated the inner electron (core) polarization and this can be included in the comparison. The total form factor can thus be described as

$$f = 0.943 f_{\text{quenched spin}} + 0.057 f_{\text{unquenched}} + f_{\text{core}}$$

with

$$f_{\text{unquenched}} = 3/5 f_{3d \text{ orbital}} + 2/5 f_{\text{unquenched } 3d \text{ spin}}$$

and

$$f_{\text{quenched spin}} = \xi \langle j_0 \rangle + \xi(5/2 \gamma - 1) A_{hkl} \langle j_4 \rangle + (1 - \xi) f_{4s \text{ spin}}$$

In this formulation, allowance has been made for the possible form factor contribution of the 4*s* conduction electrons which is determined in magnitude by the parameter ξ . With ξ defined as above, the magnetization of the 4*s* electrons M_{4s} is given in terms of the total magnetization M_t as

$$M_{4s}/M_t = 0.943(1 - \xi)$$

A second parameter γ has been introduced in the above and this defines the symmetry population of the 3*d* quenched electrons. Here,

γ represents the fractional population of the $3d$ electrons possessing E_g symmetry. The terms $\langle j_0 \rangle$ and $\langle j_4 \rangle$ are Bessel function integrals of the radial wave functions and A_{hkl} the directional coefficient as developed by Weiss and Freeman.² The $\langle j_0 \rangle$ term represents the spherical atom form factor, and the directional perturbation is included in the $\langle j_4 \rangle$ term.

It has been possible to determine the asymmetry parameter γ from a detailed study of the form factor differences relative to the spherical form factor as illustrated in Figure 1. In principle, each reflection can be used to evaluate γ , although with widely varying accuracy, and the weighted average for all reflections yields

$$\gamma = 0.53 \pm 0.01$$

Thus 53% of the $3d$ quenched electron magnetization arises from electrons with E_g symmetry and correspondingly 47% with T_{2g} symmetry. For spherical symmetry, the respective values would be 40 and 60%. It should be mentioned that the value for γ is not particularly dependent upon the selection of the spin density wave function: by using earlier wave functions of Wood and Pratt⁴ (approximate treatment of exchange polarization) one obtains a value of 0.54.

The second parameter ξ can also be determined from the form factor data. Figure 2 shows the comparison between the observed values and the total $3d$ plus core electron contributions for the case of $\xi = 1.00$, i.e., with zero $4s$ magnetization. There is seen to be a systematic discrepancy with the observed values being higher in the positive form factor region and the reverse in the negative form factor region. This difference presumably represents the influence of the $4s$ contributions to the form factor provided the $3d$ form factors calculated by Watson and Freeman are correct. Spin density distributions for the $4s$ electrons in free atoms have been given by both Wood and Pratt⁴ and Watson and Freeman.³ Form factors for these distributions have been calculated, and in either case the $4s$ form factor values over the observation region is expected to be smaller than 0.01 units, much smaller than the discrepancy shown in Figure 2. The discrepancy can be removed however by introducing ξ -values greater than unity; i.e., by introducing a negative magnetization of the $4s$ electrons. This is shown in Figure 3 and a reasonable value $\xi = 1.10$ is suggested which implies that the $4s$ electrons contribute $-0.21 \mu_B$ to the magnetization and correspondingly the total $3d$ magnetization would be $+2.39 \mu_B$. It is to be emphasized that this magnetization distribution is predicated on the acceptance of the Watson-Freeman free atom wave functions.

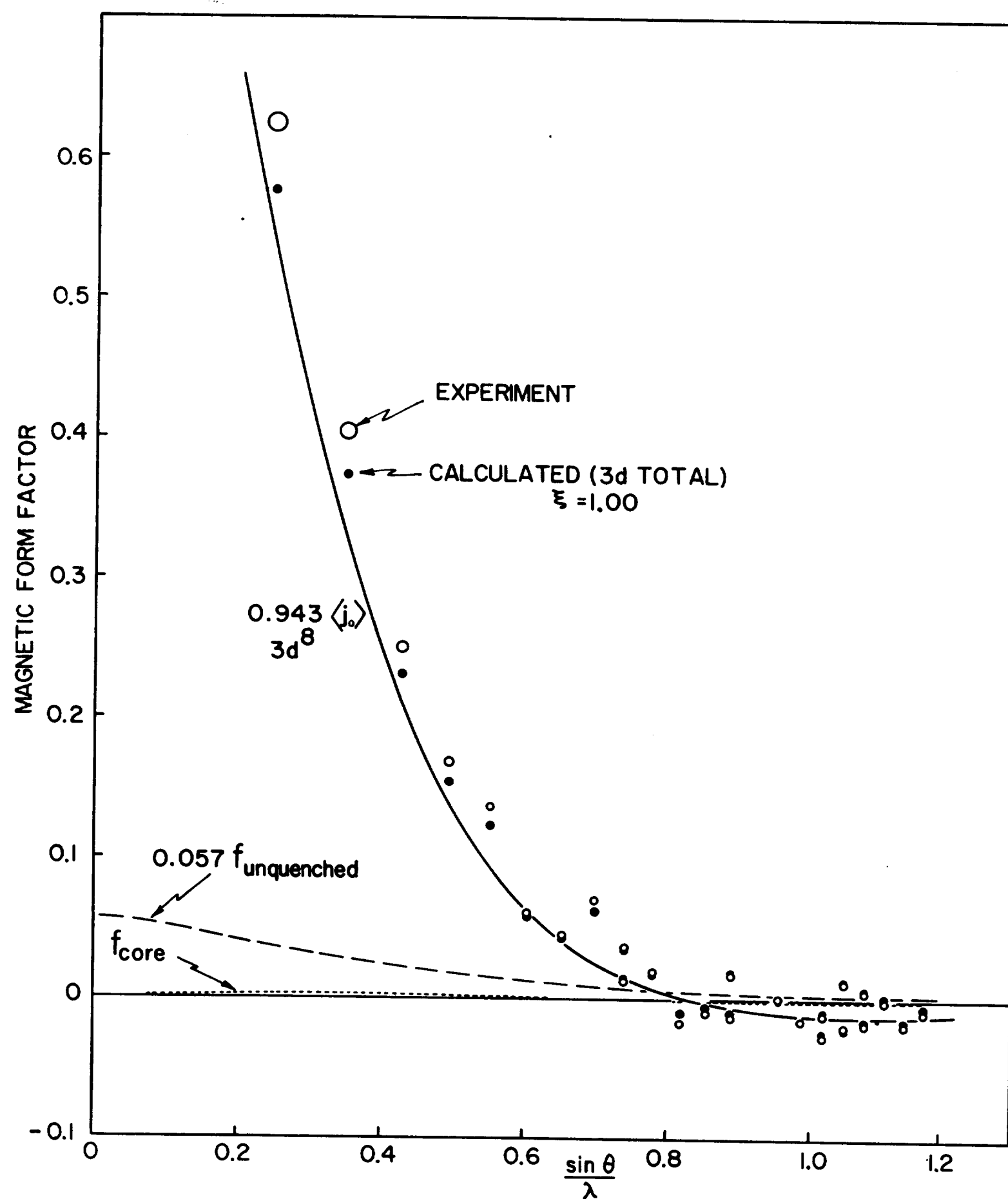


Fig. 2. Comparison between experimental and calculated values of the magnetic form factor for iron including orbital moment, core polarization, and asymmetric spin scattering. The asymmetry parameter value $\gamma = 0.53$ has been used in the calculation.

Temperature Dependence of the *d*-Shell Asymmetry

The mixture of 53% E_g and 47% T_{2g} that has been found for the directional configuration of the $3d$ quenched electrons suggested that this population ratio might be temperature dependent. Accordingly, the magnetic scattering amplitudes for two reflections, (400) and (433), which are particularly sensitive to γ , have been studied between 78 and 830°K. These reflections were selected not only because of their sensi-

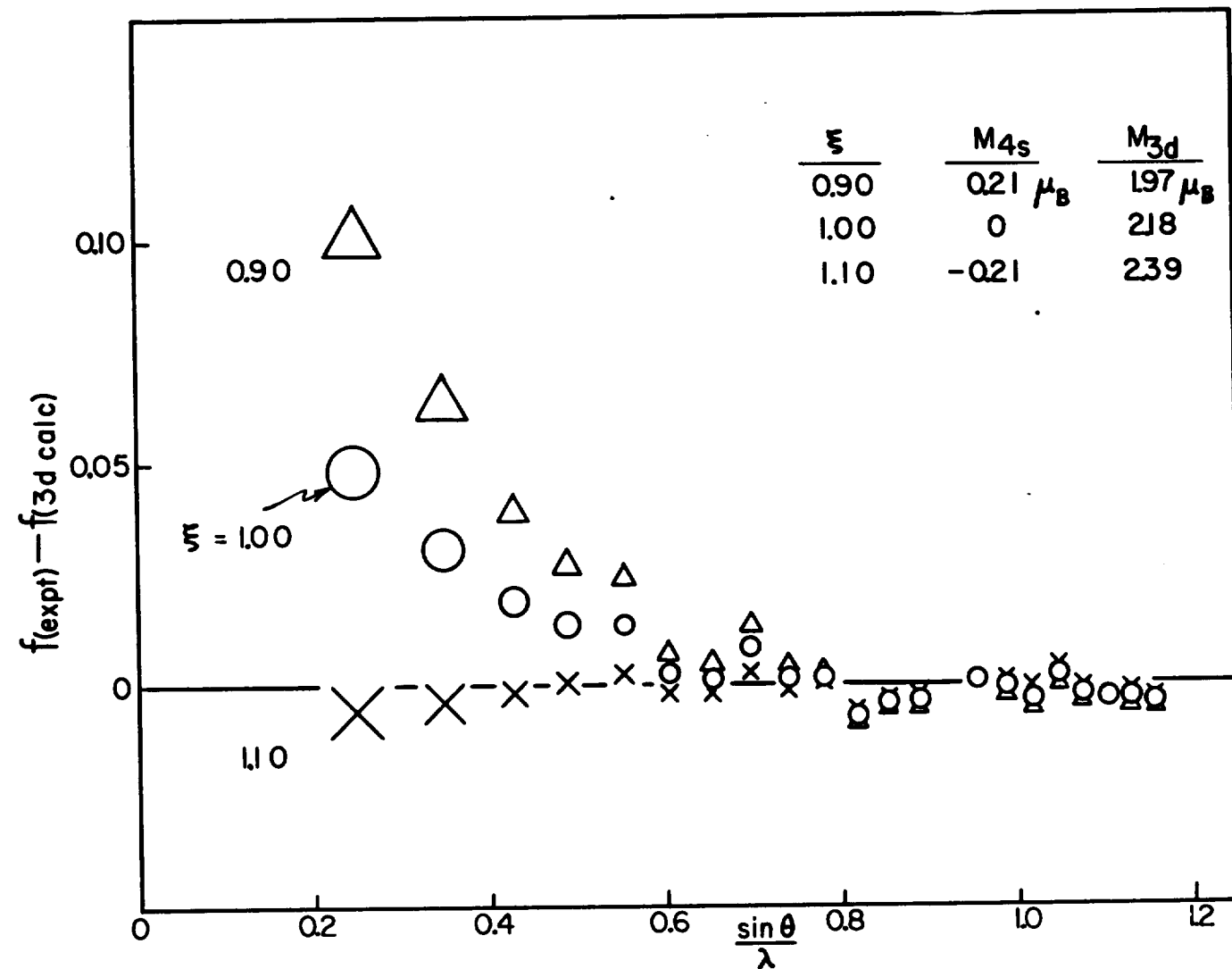


Fig. 3. Excess form factor value as a function of the 4s magnetization parameter ξ .

tivity to the directional configuration but also because they exhibit changes in the opposite direction with a configuration variation. Figure 4 illustrates the temperature dependence of the (400) magnetic scatter-

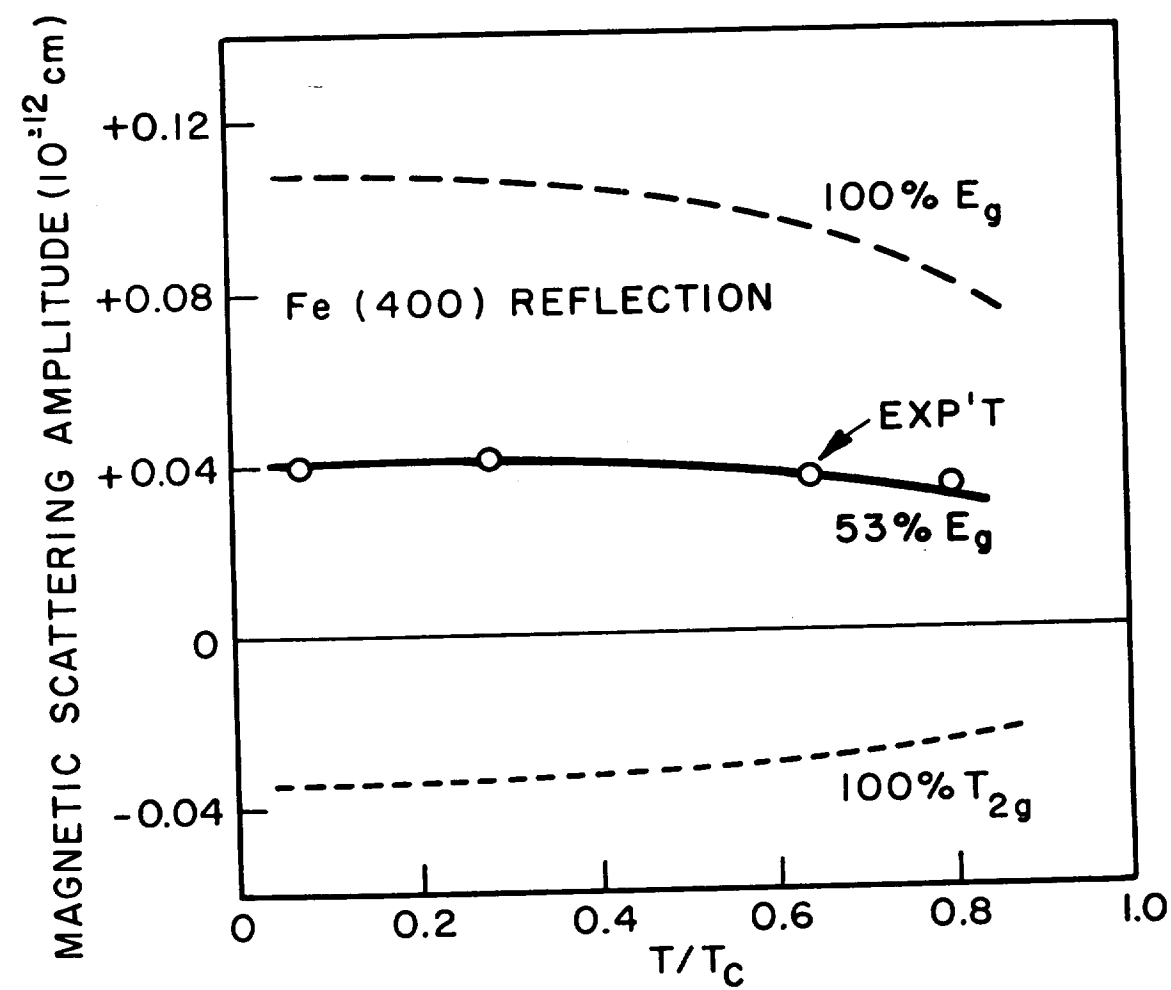


Fig. 4. Temperature dependence of the (400) magnetic scattering amplitude compared with the amplitude calculated for pure and mixed configurations.

ing amplitude along with the expected amplitude variation for the pure and mixed configurations. It is seen that very little temperature dependence is permitted and this is summarized for both reflections in Figure 5. In particular it is to be noted that there is no tendency for the spherical atom configuration to be approached at either low temperature or in the Curie temperature T_c vicinity.

Fourier Transformation of Experimental Data

The experimental data can be analyzed by Fourier transformation whereby the magnetic spin density or equivalently, the intensity of magnetization, throughout the unit cell is obtained without recourse to wave function calculations. Since all reflections out to a maximum $\sin \theta/\lambda = 1.157 \text{ \AA}^{-1}$ value were studied, three-dimensional transformation is possible. Following conventional crystallographic treatment, we have

$$\rho(xyz) = (1/V) \sum \sum \sum F_{hkl} \cos 2\pi(hx + ky + lz)$$

where $\rho(xyz)$ is the magnetic spin density or intensity of magnetization (available in absolute units of Bohr magnetons per \AA^3 or in gauss), V is the unit cell volume, and F_{hkl} is the magnetic crystal structure factor per unit cell, in the present case just twice the magnetic scattering amplitude for each reflection. The Fourier summation has been carried out on the MIT computation center IBM-709 computer and the three-dimensional density distribution has been mapped at all points in the unit cell on a grid interval of $1/60$ the unit cell edge length.

Figure 6 shows a portion of the three-dimensional map thereby ob-

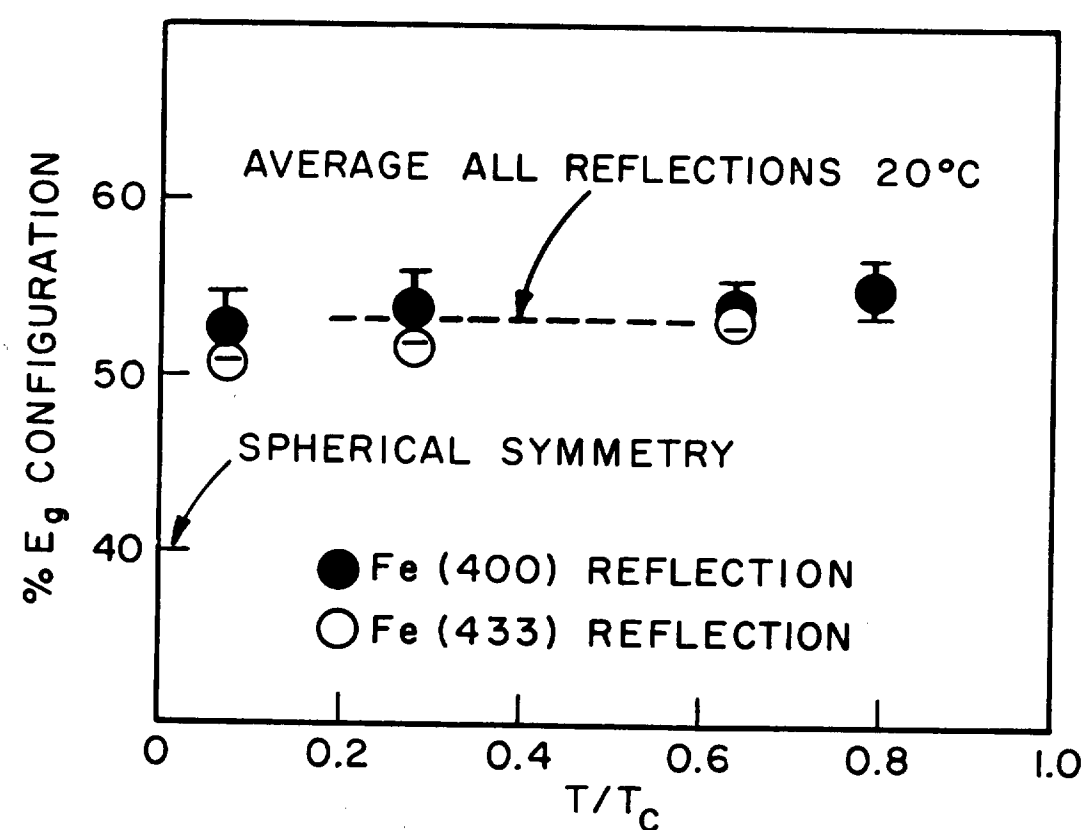


Fig. 5. Temperature dependence of the configuration asymmetry parameter γ as determined from the (400) and (433) intensity data.

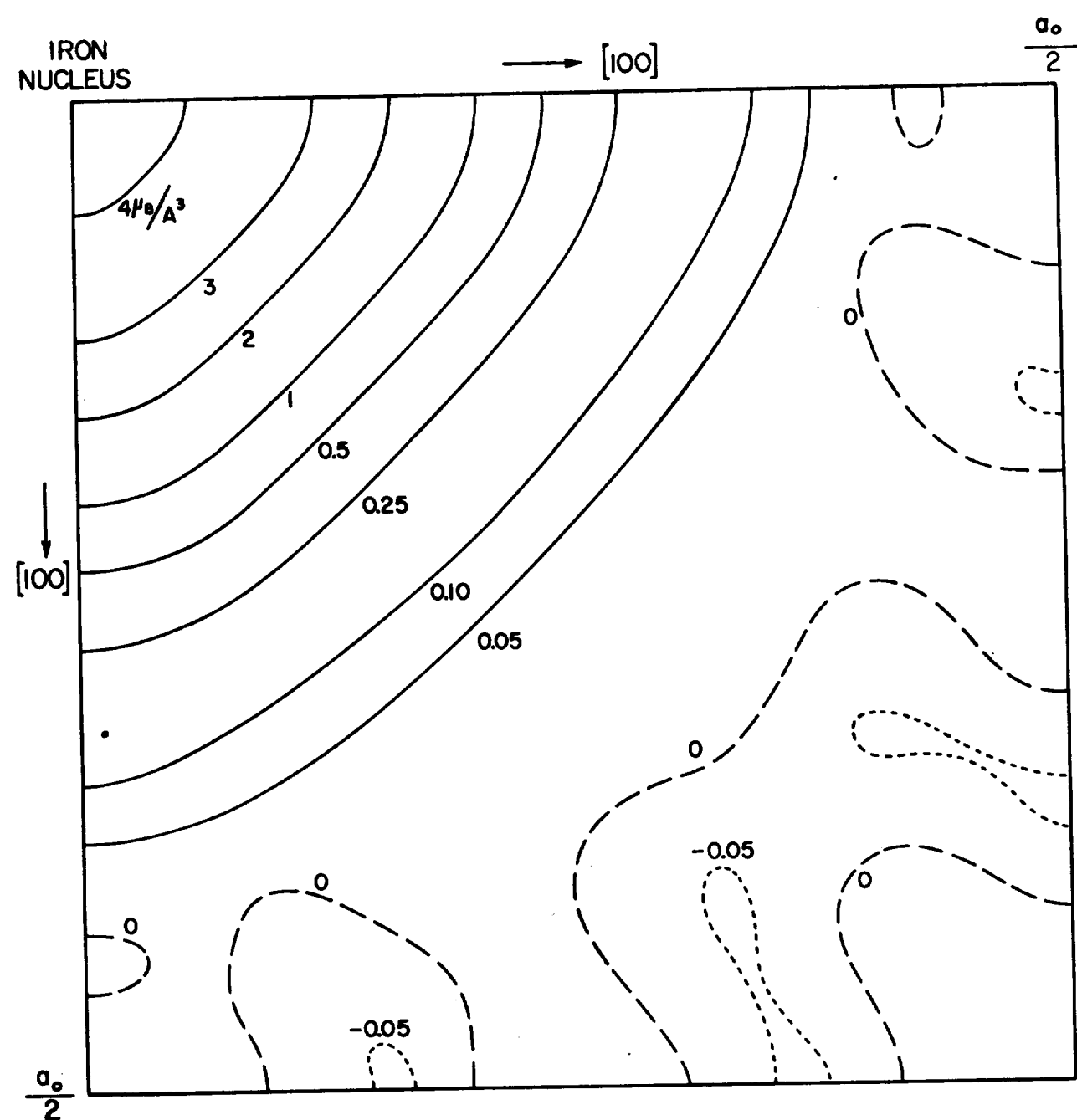


Fig. 6. Magnetic spin density distribution over the (100) face of the iron unit cell. The asymmetric contour lines show that the $3d$ electrons are asymmetrically distributed around the iron nucleus. Values for the spin density are in absolute units, Bohr magnetons per cubic angstrom.

tained for the (100) base plane of the unit cell, and Figure 7 illustrates a portion of the (110) diagonal plane intersecting the two atoms of the unit cell. It is seen that the spin density contour lines around the nuclear site in Figure 6 are not circular (as they should be for a spherical atom) but rather are compressed in the [110] direction relative to that in the [100] direction and Figure 7 suggests even higher compression in the [111] space diagonal, or nearest neighbor, direction. This is illustrated further in Figure 8 where the magnetization distribution along the three principal directions as a function of distance from the nucleus is portrayed.

These directional effects can be seen even more clearly in the equivalent maps shown in Figures 9 and 10 which represent the excess magnetic spin density over that expected from spherical symmetry. These maps were obtained by transforming the difference between F_{hkl} (experimental) and F_{hkl} (spherical calculated). In Figures 9 and 10

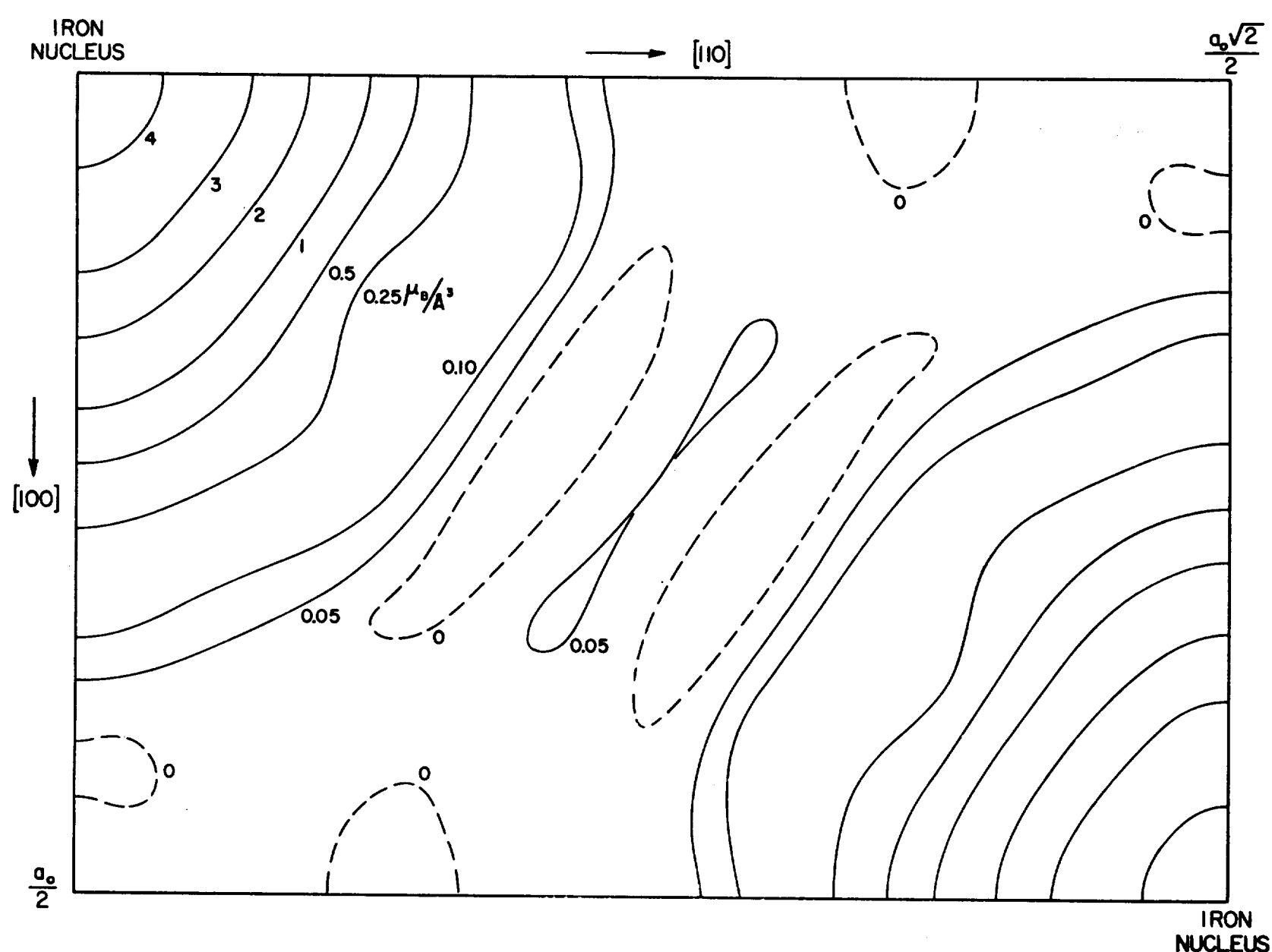


Fig. 7. Magnetic spin density distribution in the (110) diagonal plane of the iron unit cell. Two nearest neighbor iron atoms are shown in this section. Very small density is to be noted in the mid-region between these atoms.

excess density is seen in "mountainous" regions along the [100] axes, and a deficiency is exhibited in the face and space diagonal directions.

It is to be recognized that these density contour maps are representative of the true density distribution as seen with finite resolution, since data are available only to a certain maximum value of $\sin \theta/\lambda$. The limiting resolution function has been determined both by machine calculation and by theoretical analysis and is shown in Figure 8. This resolution function provides the diffraction broadening acting on any density segment because of the use of finite data. In the optical equivalent, this is the effect produced by a finite-sized viewing window. The resolution deficiency is most pronounced at small distances from the nuclear site where the spin density gradients are the largest. If the transformation is performed with data extrapolated beyond the experimental maximum of $\sin \theta/\lambda = 1.157 \text{ \AA}^{-1}$, the most pronounced effect on the maps occurs within the distance region of 0.2 or 0.3 \AA from the nuclear site. A reduction of density is obtained in this region and the distribution resembles more closely the expected $3d$ wave function

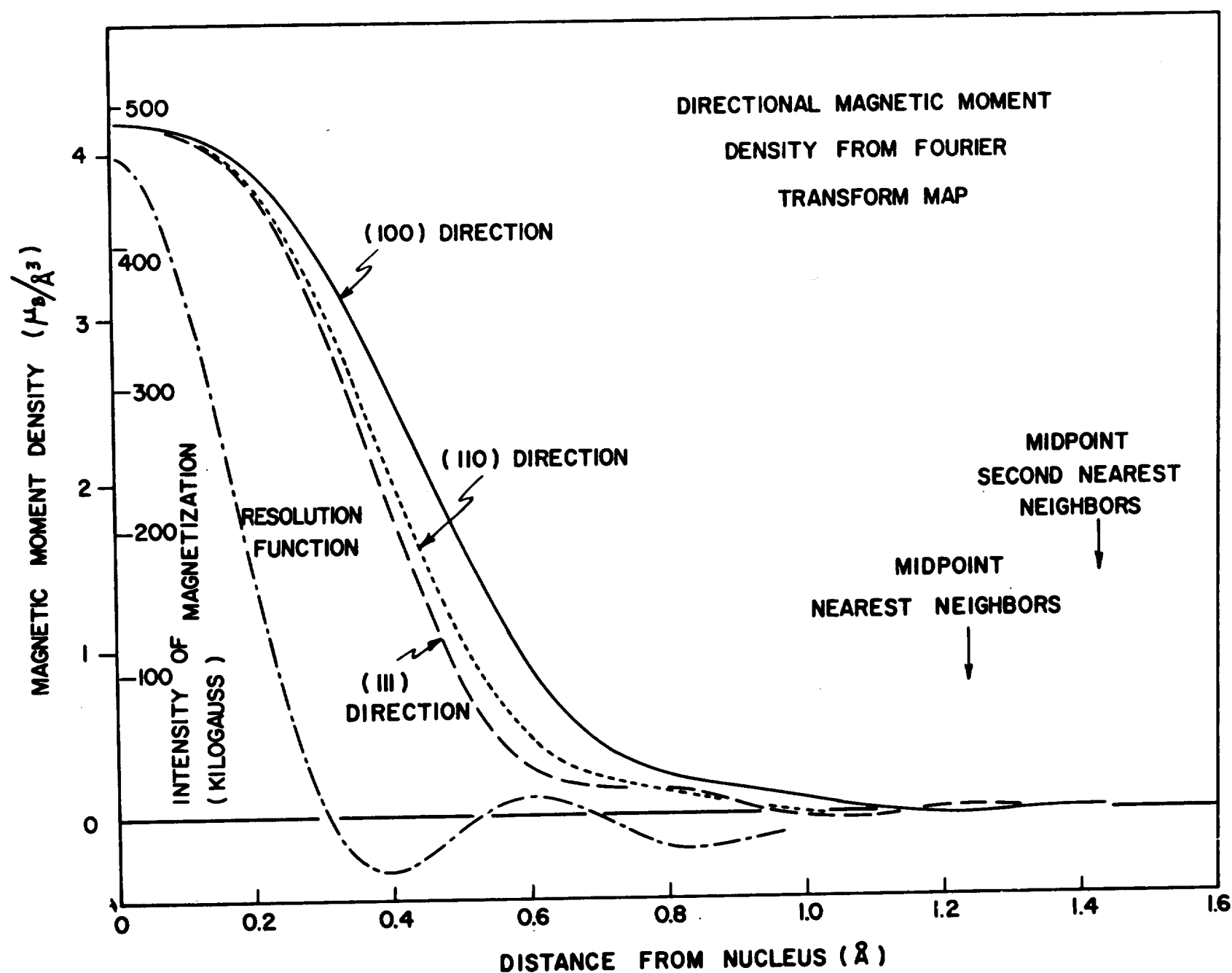


Fig. 8. Magnetic spin density variation with distance from the iron nucleus in the principal crystallographic directions. The concentration along the cube edges relative to that in the [111] direction is to be noted.

behavior. Of particular interest in the maps is the very low density which is apparent at the midpoints of the closest neighboring atoms.

Iron Atoms in Fe_3Al

Recent studies on the magnetic electron configuration of the iron atoms in Fe_3Al by Pickart and Nathans⁵ provide an interesting comparison with the above results for pure iron. In the ordered state, this alloy contains two species of iron atoms, Fe I and Fe II, in which Fe I atoms are completely surrounded by Fe II atoms in the same spatial configuration as in pure iron whereas Fe II atoms are surrounded half by Fe I atoms and half by Al atoms. Pickart and Nathans have studied the ordered alloy by the same polarized beam technique as above and have obtained accurate values for the magnetic structure amplitudes for many reflections to large scattering angle. They find that Fe I atoms possess a magnetic moment of $2.18 \mu_B$ (much the same as in pure iron) whereas Fe II atoms exhibit a lower moment of $1.50 \mu_B$. Moreover, from

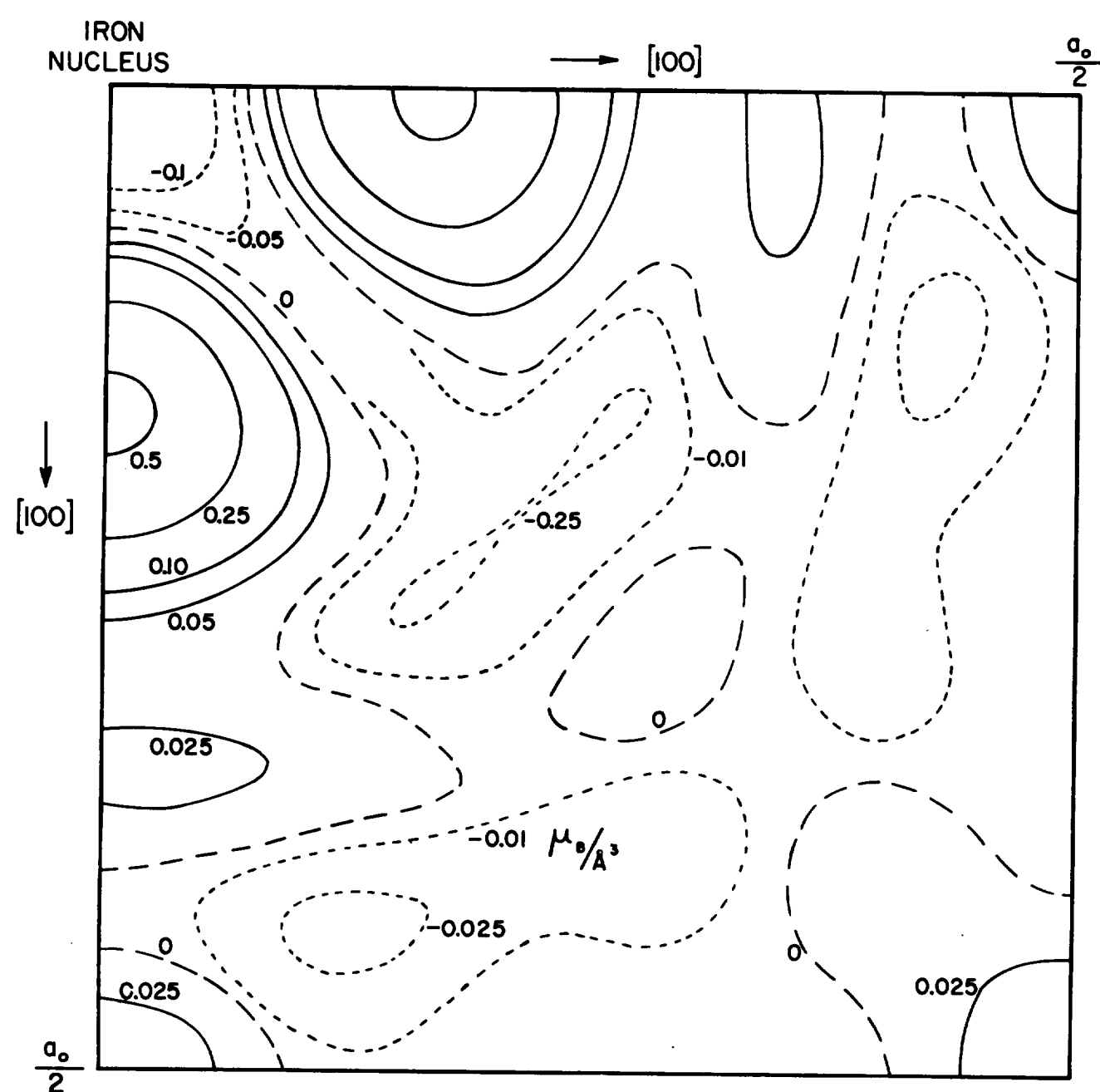


Fig. 9. Excess density in the cube face above spherically density obtained by Fourier transforming $F_{\text{expt}} - F_{\text{spher. calc.}}$. Excess density is seen along the cube edges with a deficiency along the diagonal direction.

a study of the directional character of the structure amplitudes compared to spherically symmetrical amplitudes they were able to show that Fe I atoms exhibit the mixture configuration 60% E_g - 40% T_{2g} whereas Fe II atoms are of 48% E_g - 52% T_{2g} mixture. Illustrative of the different magnetic symmetry of the two iron species is the Fourier projection map shown in Figure 11. This map represents a projection on the (110) plane of the excess scattering density over that calculated for spherically symmetrical atoms. Pronounced differences are to be seen at the different iron atom sites, and a detailed analysis of the data permits the above conclusions on the configurations.

Thus it appears that an iron atom Fe I surrounded by other iron atoms possesses closely the same magnetic configuration as in pure iron even though the surrounding iron atoms Fe II are of modified configuration. On the other hand, substitution of Al atoms for some of the surrounding iron atoms has changed the central iron atom configuration considerably.

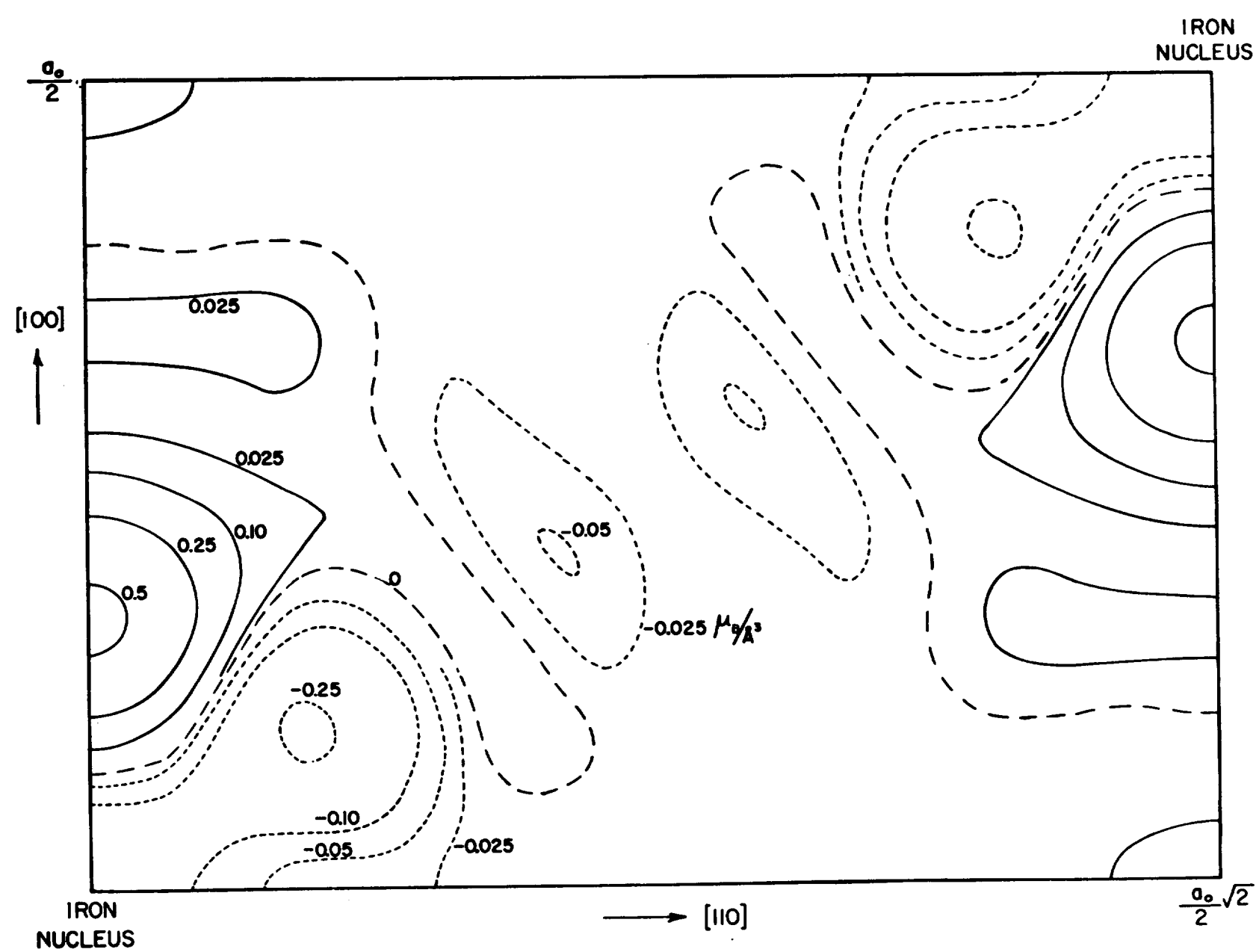


Fig. 10. Excess density in (110) diagonal plane above the spherically symmetric density. A pronounced deficiency is noted along the nearest neighbor connecting line and an excess along the cube edge.

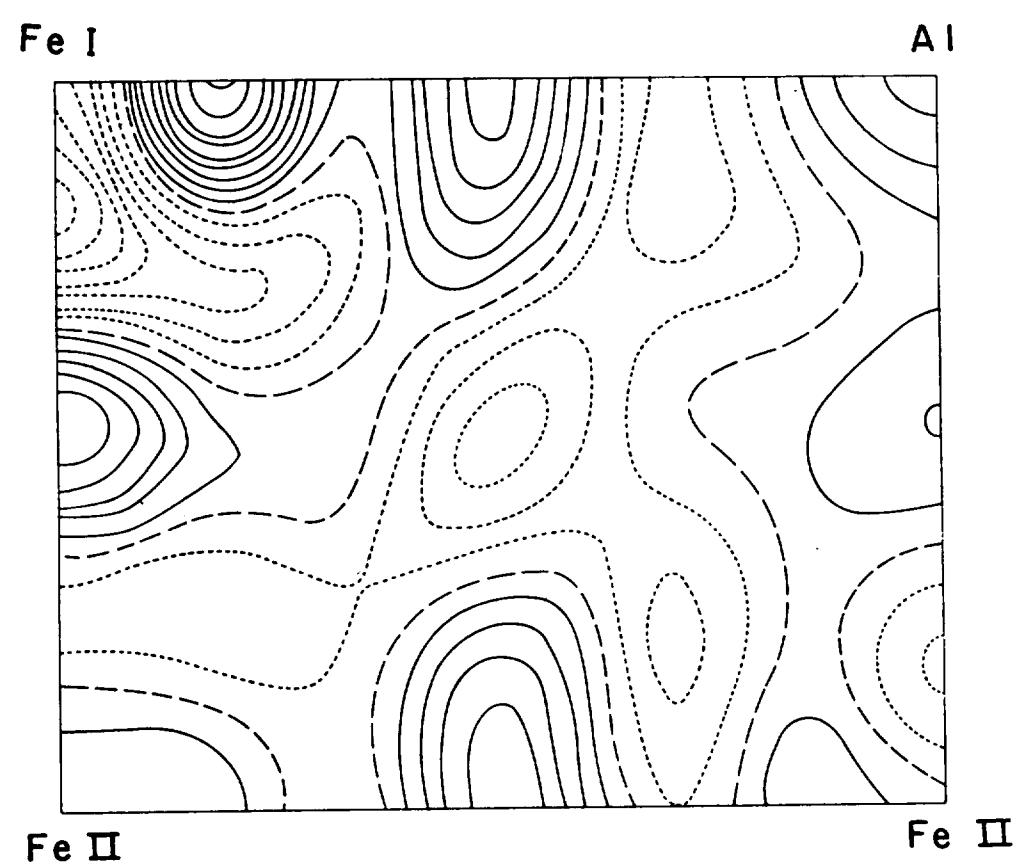


Fig. 11. Projection of excess scattering density above calculated spherical density in the (110) plane of Fe_3Al . This illustrates the different magnetic electron symmetry of the two species of iron atoms (after Pickart and Nathans).

These studies have been carried out primarily by Dr. Y. Yamada and the author with initial help by Dr. F. P. Ricci and with assistance by Dr. R. P. Ferrier in the temperature dependent studies. Mr. W. C. Phillips and Mr. R. M. Moon offered invaluable assistance in programing the computer calculations, and stimulating conversations with Dr. A. J. Freeman and Dr. R. J. Weiss are acknowledged.

References

1. Nathans, R., C. G. Shull, G. Shirane, and A. Andresen, *J. Phys. Chem. Solids*, **10**, 138 (1959).
2. Weiss, R. J., and A. J. Freeman, *J. Phys. Chem. Solids*, **10**, 147 (1959).
3. Watson, R. E., and A. J. Freeman, *Phys. Rev.*, **123**, 2027 (1961).
4. Wood, J. H., and G. W. Pratt, *Phys. Rev.*, **107**, 995 (1957).
5. Pickart, S. J., and R. Nathans, *Phys. Rev.*, **123**, 1163 (1961).